SECOND-ORDER TOTAL GENERALIZED VARIATION CONSTRAINT

Shunsuke Ono and Isao Yamada

Department of Communications and Computer Engineering, Tokyo Institute of Technology,
Meguro-ku, Tokyo 152-8550, Japan

ABSTRACT

This paper proposes to use the Total Generalized Variation (TGV) of second order in a constrained form for image processing, which we call the TGV constraint. The main contribution is twofold: i) we present a general form of convex optimization problems with the TGV constraint, which is, to the best of our knowledge, the first attempt to use TGV as a constraint and covers a wide range of problem formulations sufficient for image processing applications; and ii) a computationally-efficient algorithmic solution to the problem is provided, where we mobilize several recently-developed proximal splitting techniques to handle the complicated structured set, i.e., the TGV constraint. Experimental results illustrate the potential applicability and utility of the TGV constraint.

Index Terms— Total generalized variation (TGV), constrained optimization, epigraphical projection, proximal splitting.

1. INTRODUCTION

The *Total Variation* (TV) [1, 2], defined as the total magnitude of the vertical and horizontal discrete gradients of an image, is widely known as a standard and effective prior for images and has been successfully applied to a variety of problems arising in image processing and computer vision. Roughly speaking, there are two ways to use TV, that is, the *TV regularization* and the *TV constraint*. The TV regularization, minimizing an objective function involving TV, is much more popular than the TV constraint, minimizing an objective function while keeping TV at some level. The TV constraint, however, would be preferable in a number of cases over the TV regularization because such a constrained use of priors often facilitates parameter setting, as having been addressed, for example, in [3, 4, 5, 6], where algorithms for solving convex optimization problems with the TV constraint are also presented.

On the other hand, it is also well known that the so-called *staircasing effect*, which is the undesirable appearance of edges, accompanies the use of TV. The *Total Generalized Variation* (TGV) [7, 8] was introduced to overcome this limitation and is recognized as a well-established higher-order generalization of TV with sound theoretical properties and practical effectiveness. Indeed, the TGV of second order has recently been utilized as a regularization form in various applications [9, 10, 11, 12, 13, 14] and outperforms the TV regularization, but handling TGV in a constrained form has, to the best of our knowledge, not yet been addressed.

The above-mentioned things motivate us to develop a framework that efficiently deals with the *TGV constraint* in optimization, which is the main contribution of this paper and would increase the potential applicability and utility of TGV. To this end, first, we introduce a general form of convex optimization problems, where the sum of possibly nonsmooth convex functions is minimized over the TGV constraint (and possibly with other constraints). This formulation covers a wide range of problem formulations sufficient for image processing applications, and moreover, is designed to accept multichannel images (e.g., color images). Second, we decompose the TGV constraint into certain simpler constraints and then reformulate the problem into a certain product space expression. Finally, an efficient algorithmic solution to the reformulated problem is provided by leveraging epigraphical projection techniques [5] and a primal-dual splitting algorithm [15, 16]. The resulting algorithm requires no inner iterations. As an application, we present image restoration by using the TGV constraint with illustrative examples.

We would like to thank the anonymous reviewers for their helpful comments. This work is supported in part by JSPS Grants-in-Aid for JSPS fellows (24·2522) and (B-21300091).

2. PRELIMINARIES

In the following, $\mathbb{N}$, $\mathbb{R}$, $\mathbb{R}_+$, and $\mathbb{R}_{++}$ denote the sets of positive integers, all, nonnegative, and positive real numbers, respectively. We adopt the vector notation for multichannel images as follows: the channel components on a multichannel image of size $N_v \times N_h \times M$ ($N_v, N_h, M \in \mathbb{N}$) are stacked into a vector $\mathbf{u} := [\mathbf{u}_1^\top \cdots \mathbf{u}_M^\top]^\top \in \mathbb{R}^{MN}$ in lexicographic order, where $N = N_v N_h$ is the number of the pixels, $\mathbf{u}_m \in \mathbb{R}^N$ ($m = 1, \ldots, M$) are the channels (e.g., $M = 3$ means color images), and $\cdot^\top$ stands for the transposition. We denote the set of all proper lower semicontinuous convex functions over a Euclidean space $\mathcal{X}$ by $\Gamma_0(\mathcal{X})$, and the ℓ_2 norm by $\|\cdot\|_2$.

2.1. Total Generalized Variation

By letting $\mathbf{D}_v, \mathbf{D}_h \in \mathbb{R}^{N\times N}$ be the vertical and horizontal discrete gradient operators with Neumann boundary, the first-order discrete gradient operator for multichannel images can be expressed by $\mathbf{D} := \mathrm{diag}([\mathbf{D}_v^\top\ \mathbf{D}_h^\top]^\top, \ldots, [\mathbf{D}_v^\top\ \mathbf{D}_h^\top]^\top) \in \mathbb{R}^{2MN\times MN}$. We also introduce the following linear operator

$$\mathbf{G} := \mathrm{diag}\left(\begin{bmatrix} -\mathbf{D}_v^\top & \mathbf{O} \\ -\mathbf{D}_h^\top & -\mathbf{D}_v^\top \\ \mathbf{O} & -\mathbf{D}_h^\top \end{bmatrix}, \ldots, \begin{bmatrix} -\mathbf{D}_v^\top & \mathbf{O} \\ -\mathbf{D}_h^\top & -\mathbf{D}_v^\top \\ \mathbf{O} & -\mathbf{D}_h^\top \end{bmatrix}\right) \in \mathbb{R}^{3MN\times 2MN},$$

where $\mathbf{O}$ denotes a zero matrix of appropriate size. Moreover, define the mixed $\ell_{1,2}$ norm $\|\cdot\|_{1,2}^{(K)} : \mathbb{R}^{KN} \to \mathbb{R}_+$ by

$$\|\mathbf{z}\|_{1,2}^{(K)} := \textstyle\sum_{n=1}^N \sqrt{\sum_{k=0}^{K-1} z_{n+kN}^2} = \sum_{n=1}^N \|\mathbf{z}^{(n)}\|_2, \quad (1)$$

where $K \in \mathbb{N}$, z_i denotes the ith entry of $\mathbf{z}$, and

$$\mathbf{z}^{(n)} := [z_n\ z_{n+N} \cdots z_{n+(K-2)N}\ z_{n+(K-1)N}]^\top \in \mathbb{R}^K.$$

The *Total Generalized Variation* (TGV) of second order for multichannel images [9], denoted by $J_{\mathrm{TGV}}^\alpha : \mathbb{R}^{MN} \to \mathbb{R}_+$, is given by

$$J_{\mathrm{TGV}}^\alpha(\mathbf{u}) := \min_{\mathbf{d}\in\mathbb{R}^{2MN}} \alpha\|\mathbf{D}\mathbf{u} - \mathbf{d}\|_{1,2}^{(2M)} + (1-\alpha)\|\mathbf{G}\mathbf{d}\|_{1,2}^{(3M)},$$

where the left term corresponds to the total magnitude of the first-order vertical and horizontal discrete gradients of all channels, the right one to that of the second-order, and $\alpha \in (0,1)$ controls the balance between them.

2.2. Primal-Dual Splitting Method

A primal-dual splitting method [15, 16] brings an algorithmic solution to the following convex optimization problem: find $\mathbf{x}^\star$ in

$$\arg\min_{\mathbf{x}\in\mathcal{X}} f_1(\mathbf{x}) + f_2(\mathbf{x}) + f_3(\mathbf{L}\mathbf{x}), \tag{2}$$

where f_1 is a differentiable convex function with β-Lipschitzian gradient $\nabla f_1 : \mathcal{X} \to \mathcal{X}$ for some $\beta \in \mathbb{R}_{++}$, $f_2 \in \Gamma_0(\mathcal{X})$, $\mathbf{L} : \mathcal{X} \to \mathcal{Y}$ is a linear operator ($\mathcal{Y}$ is another Euclidean space), and $f_3 \in \Gamma_0(\mathcal{Y})$. The algorithm is given by

$$\left\lfloor \begin{array}{l} \mathbf{x}^{(n+1)} = \mathrm{prox}_{\gamma_1 f_2}[\mathbf{x}^{(n)} - \gamma_1(\nabla f_1(\mathbf{x}^{(n)}) + \mathbf{L}^*\mathbf{y}^{(n)})], \\ \mathbf{y}^{(n+1)} = \mathrm{prox}_{\gamma_2 f_3^*}[\mathbf{y}^{(n)} + \gamma_2\mathbf{L}(2\mathbf{x}^{(n+1)} - \mathbf{x}^{(n)})], \end{array}\right. \tag{3}$$

where prox denotes the *proximity operator*[1], f_3^* the *Fenchel-Rockafellar conjugate function*[2] of f_3, $\mathbf{L}^*$ the adjoint operator of $\mathbf{L}$, and $\gamma_1, \gamma_2 \in \mathbb{R}_{++}$ satisfy $\gamma_1^{-1} - \gamma_2\|\mathbf{L}\|_{op}^2 \geq \frac{\beta}{2}$ ($\|\cdot\|_{op}$ stands for the operator norm). Under some mild conditions, the sequence $(\mathbf{x}^{(n)})_{n\in\mathbb{N}}$ converges to a solution to (2).

3. PROPOSED FRAMEWORK

3.1. Problem Formulation

For arbitrary chosen $\mu \in \mathbb{R}_+$ and $\alpha \in (0,1)$, we newly define the *TGV constraint* as follows:

$$C_{\mathrm{TGV}}^{\alpha,\mu} := \{(\mathbf{u},\mathbf{d}) \in \mathbb{R}^{MN} \times \mathbb{R}^{2MN} |\ \alpha\|\mathbf{D}\mathbf{u} - \mathbf{d}\|_{1,2}^{(2M)} + (1-\alpha)\|\mathbf{G}\mathbf{d}\|_{1,2}^{(3M)} \leq \mu\},$$

which is evidently a nonempty closed convex set. Our target convex optimization problem with the TGV constraint is then formulated as follows: find $(\mathbf{u}^\star, \mathbf{d}^\star)$ in

$$\arg\min_{\mathbf{u},\mathbf{d}} \varphi(\mathbf{u},\mathbf{d}) + \sum_{s=1}^{S} \psi_s(\mathbf{L}_s\mathbf{u}, \mathbf{P}_s\mathbf{d}) \text{ s.t. } \begin{cases} \mathbf{u} \in [\underline{\omega}, \overline{\omega}]^{MN}, \\ (\mathbf{u},\mathbf{d}) \in C_{\mathrm{TGV}}^{\alpha,\mu}, \end{cases} \tag{4}$$

where $\varphi : \mathbb{R}^{3MN} \to \mathbb{R}$ is a differentiable convex function with β-Lipschitzian gradient $\nabla\varphi : \mathbb{R}^{MN} \to \mathbb{R}^{MN}$ for some $\beta \in \mathbb{R}_{++}$, $\mathbf{L}_s \in \mathbb{R}^{L_s \times MN}$ and $\mathbf{P}_s \in \mathbb{R}^{P_s \times MN}$ ($s = 1, \ldots, S$) are matrices, $\psi_s \in \Gamma_0(\mathbb{R}^{L_s+P_s})$ ($s = 1, \ldots, S$), and $[\underline{\omega}, \overline{\omega}]^{MN}$ is a numerical range constraint with $\underline{\omega}, \overline{\omega} \in \mathbb{R}$ ($\underline{\omega} \leq \overline{\omega}$). Here we assume that the proximity operators of ψ_s ($s = 1, \ldots, S$) are computable.

Proposition 3.1. *Suppose that* $[\underline{\omega}, \overline{\omega}]^{MN} \times \mathbb{R}^{2MN} \cap C_{\mathrm{TGV}}^{\alpha,\mu} \neq \emptyset$. *Then* (4) *has at least one solution.*

Proof. By using the indicator functions[3] of $[\underline{\omega}, \overline{\omega}]^{MN}$ and $C_{\mathrm{TGV}}^{\alpha,\mu}$, (4) can be rewritten as

$$\min_{\mathbf{u},\mathbf{d}} \varphi(\mathbf{u},\mathbf{d}) + \textstyle\sum_{s=1}^{S} \psi_s(\mathbf{L}_s\mathbf{u}, \mathbf{P}_s\mathbf{d}) + \iota_{[\underline{\omega},\overline{\omega}]^{MN}}(\mathbf{u}) + \iota_{C_{\mathrm{TGV}}^{\alpha,\mu}}(\mathbf{u},\mathbf{d}). \tag{5}$$

Then we only need to check the coercivity[4] of (5). If $\|\mathbf{u}\|_2 \to \infty$ then $\iota_{[\underline{\omega},\overline{\omega}]^{MN}}(\mathbf{u}) \to \infty$, else if $\|\mathbf{d}\|_2 \to \infty$ then $\iota_{C_{\mathrm{TGV}}^{\alpha,\mu}}(\mathbf{u},\mathbf{d}) \to \infty$, which completes the proof. □

Remark 3.1 (Other constraints)**.** One can impose other convex constraints to (4) via their indicator functions. Specifically, for any closed convex set C (the metric projection onto it is computable) and for any pair of matrices $\mathbf{M}_1$ and $\mathbf{M}_2$, imposing $(\mathbf{M}_1\mathbf{u}, \mathbf{M}_2\mathbf{d}) \in C$ to (4) can be realized by assigning $\psi_s := \iota_C$, $\mathbf{L}_s := \mathbf{M}_1$, and $\mathbf{P}_s := \mathbf{M}_2$.

3.2. Optimization

In what follows, we reformulate (4) to solve it by (3) with the help of epigraphical projection techniques [5]. The main computational difficulty stems from the fact that the metric projection onto the TGV constraint is unavailable (see footnote 3 for the definition of the metric projection). To circumvent this, first, we give another expression of the TGV constraint as follows:

$$(\mathbf{u},\mathbf{d}) \in C_{\mathrm{TGV}}^{\alpha,\mu} \Leftrightarrow (\mathbf{D}\mathbf{u} - \mathbf{d}, \mathbf{G}\mathbf{d}) \in C_{1,2}^{\alpha,\mu}, \tag{6}$$

where

$$C_{1,2}^{\alpha,\mu} := \{(\mathbf{z}_1,\mathbf{z}_2) \in \mathbb{R}^{(2+3)MN} |\ \alpha\|\mathbf{z}_1\|_{1,2}^{(2M)} + (1-\alpha)\|\mathbf{z}_2\|_{1,2}^{(3M)} \leq \mu\}.$$

Second, we introduce the following two closed convex sets:

$$C_{\mathrm{epi},\ell_2}^{K,w} := \{(\mathbf{z}, \boldsymbol{\zeta}) \in \mathbb{R}^{KN} \times \mathbb{R}^{N} |\ w\|\mathbf{z}^{(n)}\|_2 \leq \zeta_n,\ n = 1, \ldots, N\}, \tag{7}$$

$$C_{\mathrm{hs}}^{\mu} := \{(\boldsymbol{\zeta}_1, \boldsymbol{\zeta}_2) \in \mathbb{R}^{N} \times \mathbb{R}^{N} |\ \textstyle\sum_{i=1}^{2} \langle \mathbf{1}_N, \boldsymbol{\zeta}_i \rangle \leq \mu\}, \tag{8}$$

where $w \in \mathbb{R}_{++}$, ζ_n is the nth entry of $\boldsymbol{\zeta}$, and $\mathbf{1}_N := [1 \cdots 1]^\top \in \mathbb{R}^N$ (see (1) for the definition of $\mathbf{z}^{(n)}$). As will be explained, the metric projection onto (7) is computable by epigraphical projection techniques. Meanwhile, (8) is a closed half space, the metric projection onto which can also be computed. Then, we can decompose the right inclusion in (6) into three inclusions via the above sets and the auxiliary variables $\boldsymbol{\eta}_1, \boldsymbol{\eta}_2$, as follows:

$$(\mathbf{D}\mathbf{u} - \mathbf{d}, \mathbf{G}\mathbf{d}) \in C_{1,2}^{\alpha,\mu} \Leftrightarrow \begin{cases} (\mathbf{D}\mathbf{u} - \mathbf{d}, \boldsymbol{\eta}_1) \in C_{\mathrm{epi},\ell_2}^{2M,\alpha}, \\ (\mathbf{G}\mathbf{d}, \boldsymbol{\eta}_2) \in C_{\mathrm{epi},\ell_2}^{3M,1-\alpha}, \\ (\boldsymbol{\eta}_1, \boldsymbol{\eta}_2) \in C_{\mathrm{hs}}^{\mu}, \end{cases} \tag{9}$$

which translates the TGV constraint into simpler sets, the metric projections onto which are available. Our target problem is finally reformulated as follows: find $(\mathbf{u}^\star, \mathbf{d}^\star)$ in

$$\arg\min_{\mathbf{u},\mathbf{d},\boldsymbol{\eta}_1,\boldsymbol{\eta}_2} \varphi(\mathbf{u},\mathbf{d}) + \textstyle\sum_{s=1}^{S} \psi_s(\mathbf{L}_s\mathbf{u}, \mathbf{P}_s\mathbf{d}) \text{ s.t. } \begin{cases} \mathbf{u} \in [\underline{\omega}, \overline{\omega}]^{MN}, \\ (\mathbf{D}\mathbf{u} - \mathbf{d}, \boldsymbol{\eta}_1) \in C_{\mathrm{epi},\ell_2}^{2M,\alpha}, \\ (\mathbf{G}\mathbf{d}, \boldsymbol{\eta}_2) \in C_{\mathrm{epi},\ell_2}^{3M,1-\alpha}, \\ (\boldsymbol{\eta}_1, \boldsymbol{\eta}_2) \in C_{\mathrm{hs}}^{\mu}. \end{cases} \tag{10}$$

Now, by letting

$$\mathbf{L} := \begin{bmatrix} \mathbf{D} & -\mathbf{I} & \mathbf{O} & \mathbf{O} \\ \mathbf{O} & \mathbf{O} & \mathbf{I} & \mathbf{O} \\ \mathbf{O} & \mathbf{G} & \mathbf{O} & \mathbf{O} \\ \mathbf{O} & \mathbf{O} & \mathbf{O} & \mathbf{I} \\ \mathbf{L}_1 & \mathbf{P}_1 & \mathbf{O} & \mathbf{O} \\ \vdots & \vdots & \vdots & \vdots \\ \mathbf{L}_S & \mathbf{P}_S & \mathbf{O} & \mathbf{O} \end{bmatrix}, \mathbf{x} := \begin{bmatrix} \mathbf{u} \\ \mathbf{d} \\ \boldsymbol{\eta}_1 \\ \boldsymbol{\eta}_2 \end{bmatrix}, \mathbf{y} := \begin{bmatrix} \mathbf{z}_1 \\ \boldsymbol{\zeta}_1 \\ \mathbf{z}_2 \\ \boldsymbol{\zeta}_2 \\ \boldsymbol{\xi}_1 \\ \vdots \\ \boldsymbol{\xi}_S \end{bmatrix}$$

$$f_1(\mathbf{x}) := \varphi(\mathbf{u},\mathbf{d}),\ f_2(\mathbf{x}) := \iota_{[\underline{\omega},\overline{\omega}]^{MN}}(\mathbf{u}) + \iota_{C_{\mathrm{hs}}^{\mu}}(\boldsymbol{\eta}_1, \boldsymbol{\eta}_2), \text{ and}$$

$$f_3(\mathbf{y}) := \iota_{C_{\mathrm{epi},\ell_2}^{2M,\alpha}}(\mathbf{z}_1, \boldsymbol{\zeta}_1) + \iota_{C_{\mathrm{epi},\ell_2}^{3M,1-\alpha}}(\mathbf{z}_2, \boldsymbol{\zeta}_2) + \textstyle\sum_{s=1}^{S} \psi_s(\boldsymbol{\xi}_s),$$

(10) can be seen as (2), where $\mathbf{I}$ denotes identity matrices of appropriate size. The gradient of f_1 is equivalent to that of φ, and the computation of the proximity operators of f_2 and f_3 can be decoupled with respect to each function in f_2 and f_3 because the supports of the variables corresponding to each function are separable. This structure makes it possible to solve (2) with the above settings, i.e.,

[1] The *proximity operator* [17] of a function $f \in \Gamma_0(\mathcal{X})$ of an index $\gamma \in \mathbb{R}_{++}$ is defined by $\mathrm{prox}_{\gamma f}(\mathbf{x}) := \arg\min_{\mathbf{y}\in\mathcal{X}} f(\mathbf{y}) + \frac{1}{2\gamma}\|\mathbf{x} - \mathbf{y}\|_2^2$.

[2] The *Fenchel-Rockafellar conjugate function* of $f \in \Gamma_0(\mathcal{H})$ is defined by $f^*(\boldsymbol{\xi}) := \sup_{\mathbf{x}\in\mathcal{H}}\{\langle \mathbf{x}, \boldsymbol{\xi}\rangle - f(\mathbf{x})\}$. The proximity operator of f^* can be expressed as $\mathrm{prox}_{\gamma f^*}(\mathbf{x}) = \mathbf{x} - \gamma\mathrm{prox}_{\gamma^{-1} f}(\gamma^{-1}\mathbf{x})$.

[3] For any closed convex set $C \in \mathcal{X}$, the *indicator function* of C is defined by $\iota_C(\mathbf{x}) := 0$, if $\mathbf{x} \in C$; ∞, otherwise. The proximity operator of ι_C is equivalent to the *metric projection* onto C, i.e., $\mathrm{prox}_{\gamma\iota_C}(\mathbf{x}) = \arg\min_{\mathbf{y}\in C}\|\mathbf{x} - \mathbf{y}\| =: P_C(\mathbf{x})$ ($\forall\gamma \in \mathbb{R}_{++}$).

[4] A function $f \in \Gamma_0(\mathcal{X})$ is called *coercive* if $\|\mathbf{x}\|_2 \to \infty \Rightarrow f(\mathbf{x}) \to \infty$. In this case, the existence of a minimizer of f is guaranteed, that is, there exists $\mathbf{x}^\star \in \mathrm{dom}(f)$ such that $f(\mathbf{x}^\star) = \inf_{\mathbf{x}\in\mathcal{X}} f(\mathbf{x})$.

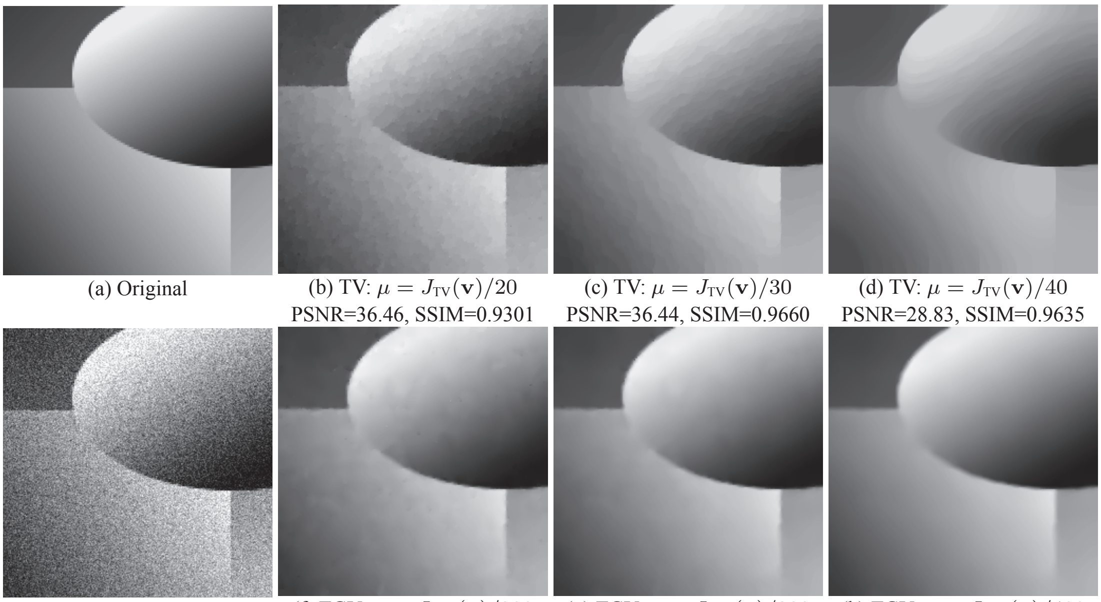

(a) Original

(b) TV: $\mu = J_{\text{TV}}(\mathbf{v})/20$ PSNR=36.46, SSIM=0.9301

(c) TV: $\mu = J_{\text{TV}}(\mathbf{v})/30$ PSNR=36.44, SSIM=0.9660

(d) TV: $\mu = J_{\text{TV}}(\mathbf{v})/40$ PSNR=28.83, SSIM=0.9635

(e) Noisy

(f) TGV: $\mu = J_{\text{TGV}}(\mathbf{v})/200$ PSNR=37.42, SSIM=0.9773

(g) TGV: $\mu = J_{\text{TGV}}(\mathbf{v})/300$ PSNR=37.35, SSIM=0.9827

(h) TGV: $\mu = J_{\text{TGV}}(\mathbf{v})/400$ PSNR=35.93, SSIM=0.9797

Fig. 1. Gaussian denoising results using a grayscale synthesized image.

(10), by (3), resulting in Algorithm 3.1 (see also footnote 2), where $\nabla^{\mathbf{u}}\varphi$ and $\nabla^{\mathbf{d}}\varphi$ denote the gradients of φ with respect to $\mathbf{u}$ and $\mathbf{d}$, respectively. The computations of the metric projections required in the algorithm are summarized in the following remark.

Remark 3.2 (Computations of metric projections)**.**

- $P_{[\underline{\omega},\overline{\omega}]^{MN}}$ is simply calculated by pushing each entry into $[\underline{\omega},\overline{\omega}]$.
- $P_{C^{K,w}_{\text{epi},\ell_2}}$ can be computed by using [5, Corollary 3.2] as follows: $P_{C^{K,w}_{\text{epi},\ell_2}}(\mathbf{z},\boldsymbol{\zeta}) = (\tilde{\mathbf{z}},\tilde{\boldsymbol{\zeta}})$, where, for $n = 1,\ldots,N$, $(\tilde{\mathbf{z}}^{(n)},\tilde{\zeta}_n) :=$
$$\begin{cases} (\mathbf{0},0), & \text{if } \|\mathbf{z}^{(n)}\|_2 < -w\zeta_n, \\ (\mathbf{z}^{(n)},\zeta_n), & \text{if } \|\mathbf{z}^{(n)}\|_2 < \frac{\zeta_n}{w}, \\ \frac{1}{1+w^2}\left(1+\frac{w\zeta_n}{\|\mathbf{z}^{(n)}\|_2}\right)(\mathbf{z}^{(n)}, w\|\mathbf{z}^{(n)}\|_2), & \text{otherwise.} \end{cases}$$
- $P_{C^{\mu}_{\text{hs}}}$ is given by [18, (3.3-10)]: $P_{C^{\mu}_{\text{hs}}}(\mathbf{x}) := \mathbf{x}$, if $\langle \mathbf{1}_N, \mathbf{x}\rangle \leq \mu$; $\mathbf{x} + \frac{\mu - \langle \mathbf{1}_N,\mathbf{x}\rangle}{N}\mathbf{1}_N$, otherwise.

Algorithm 3.1 Solver for (4)

Set $n = 0$ and choose $\mathbf{u}^{(0)}, \mathbf{d}^{(0)}, \boldsymbol{\eta}_i^{(0)}, \mathbf{z}_i^{(0)}, \boldsymbol{\zeta}_i^{(0)} (i = 1,2), \boldsymbol{\xi}_s^{(0)} (s = 1,\ldots,S), \gamma_1, \gamma_2$.

while a stop criterion is not satisfied **do**

$\bar{\mathbf{u}}^{(n)} = \mathbf{u}^{(n)} - \gamma_1(\nabla^{\mathbf{u}}\varphi(\mathbf{u}^{(n)},\mathbf{d}^{(n)}) + \mathbf{D}^\top \mathbf{z}_1^{(n)} + \sum_{s=1}^S \mathbf{L}_s^\top \boldsymbol{\xi}_s^{(n)})$

$\mathbf{u}^{(n+1)} = P_{[\underline{\omega},\overline{\omega}]^{MN}}(\bar{\mathbf{u}}^{(n)})$

$\mathbf{d}^{(n+1)} = \mathbf{d}^{(n)} - \gamma_1(\nabla^{\mathbf{d}}\varphi(\mathbf{u}^{(n)},\mathbf{d}^{(n)}) - \mathbf{z}_1^{(n)} + \mathbf{G}^\top \mathbf{z}_2^{(n)} + \sum_{s=1}^S \mathbf{P}_s^\top \boldsymbol{\xi}_s^{(n)})$

$\bar{\boldsymbol{\eta}}_i^{(n)} = \boldsymbol{\eta}_i^{(n)} - \gamma_1 \boldsymbol{\zeta}_i \quad (\forall i = 1,2)$

$(\boldsymbol{\eta}_1^{(n+1)}, \boldsymbol{\eta}_2^{(n+1)}) = P_{C^{\mu}_{\text{hs}}}(\bar{\boldsymbol{\eta}}_1^{(n)}, \bar{\boldsymbol{\eta}}_2^{(n)})$

$\bar{\mathbf{z}}_1^{(n)} = \mathbf{z}_1^{(n)} + \gamma_2(\mathbf{D}(2\mathbf{u}^{(n+1)} - \mathbf{u}^{(n)}) - 2(\mathbf{d}^{(n+1)} - \mathbf{d}^{(n)}))$

$\bar{\mathbf{z}}_2^{(n)} = \mathbf{z}_2^{(n)} + \gamma_2 \mathbf{G}(2\mathbf{d}^{(n+1)} - \mathbf{d}^{(n)})$

$\bar{\boldsymbol{\zeta}}_i^{(n)} = \boldsymbol{\zeta}_i^{(n)} + \gamma_2(2\boldsymbol{\eta}_i^{(n+1)} - \boldsymbol{\eta}_i^{(n)}) \quad (\forall i = 1,2)$

$\bar{\boldsymbol{\xi}}_s^{(n)} = \boldsymbol{\xi}_s^{(n)} + \gamma_2(\mathbf{L}_s(2\mathbf{u}^{(n+1)} - \mathbf{u}^{(n)}) + \mathbf{P}_s(2\mathbf{d}^{(n+1)} - \mathbf{d}^{(n)})) \quad (\forall s = 1,\ldots,S)$

$(\mathbf{z}_1^{(n+1)}, \boldsymbol{\zeta}_1^{(n+1)}) = (\bar{\mathbf{z}}_1^{(n)}, \bar{\boldsymbol{\zeta}}_1^{(n)}) - \gamma_2 P_{C^{2M,\alpha}_{\text{epi},\ell_2}}(\frac{1}{\gamma_2}\bar{\mathbf{z}}_1^{(n)}, \frac{1}{\gamma_2}\bar{\boldsymbol{\zeta}}_1^{(n)})$

$(\mathbf{z}_2^{(n+1)}, \boldsymbol{\zeta}_2^{(n+1)}) = (\bar{\mathbf{z}}_2^{(n)}, \bar{\boldsymbol{\zeta}}_2^{(n)}) - \gamma_2 P_{C^{3M,1-\alpha}_{\text{epi},\ell_2}}(\frac{1}{\gamma_2}\bar{\mathbf{z}}_2^{(n)}, \frac{1}{\gamma_2}\bar{\boldsymbol{\zeta}}_2^{(n)})$

$\boldsymbol{\xi}_s^{(n+1)} = \bar{\boldsymbol{\xi}}_s^{(n)} - \gamma_2 \text{prox}_{\frac{1}{\gamma_2}\psi_s}(\frac{1}{\gamma_2}\bar{\boldsymbol{\xi}}_s^{(n)}) \quad (\forall s = 1,\ldots,S)$

$n = n+1$

end while

Output $\mathbf{u}^{(n)}$

3.3. Application to Image Restoration

Consider the following observation model:

$$\mathbf{v} = \mathbf{\Phi}\mathbf{u}_{\text{org}} + \mathbf{n}_\sigma \tag{11}$$

where $\mathbf{v} \in \mathbb{R}^L$ (L and MN may be different) is an observation, $\mathbf{u}_{\text{org}} \in \mathbb{R}^{MN}$ an unknown clean image we wish to estimate, $\mathbf{\Phi} \in \mathbb{R}^{L\times MN}$ a linear operator representing some degradation (e.g., blur), and $\mathbf{n}_\sigma \in \mathbb{R}^L$ is an additive white Gaussian noise with standard deviation $\sigma \in \mathbb{R}_+$. Image restoration by using the TGV constraint under (11) is formulated as follows: find $(\mathbf{u}^\star, \mathbf{d}^\star)$ in

$$\arg\min_{\mathbf{u}} \tfrac{1}{2}\|\mathbf{\Phi}\mathbf{u} - \mathbf{v}\|_2^2 \quad \text{s.t.} \begin{cases} \mathbf{u} \in [0,255]^{MN}, \\ (\mathbf{u},\mathbf{d}) \in C^{\alpha,\mu}_{\text{TGV}}, \end{cases} \tag{12}$$

where the objective function is the standard ℓ_2 data-fidelity for a Gaussian noise contamination, and $[0,255]^{MN}$ represents the numerical range of eight-bit images. This formulation corresponds to maximize the likelihood of $\mathbf{u}$ while keeping a reasonably low TGV, expected to result in an effective restoration.

By letting $\varphi(\mathbf{u},\mathbf{d}) := \frac{1}{2}\|\mathbf{\Phi}\mathbf{u} - \mathbf{v}\|_2^2$, $\psi_s(\mathbf{L}_s\mathbf{u}, \mathbf{P}_s\mathbf{d}) = 0$ ($s = 1,\ldots,S$), and $[\underline{\omega},\overline{\omega}] := [0,255]$, (4) is reduced to (12), so that we can solve (12) by Algorithm 3.1, where $\nabla\varphi^{\mathbf{u}}(\mathbf{u},\mathbf{d}) = \mathbf{\Phi}^\top(\mathbf{\Phi}\mathbf{u} - \mathbf{v})$ and $\nabla\varphi^{\mathbf{d}}(\mathbf{u},\mathbf{d}) = \mathbf{0}$.

4. EXPERIMENTAL RESULTS

We have examined how the TGV constraint performs compared to the TV constraint in several restoration problems.[5] For solv-

[5] The experiments do not aim to give a state-of-the-art restoration performance, but concentrates on demonstrating how the TGV constraint acts. Although the use of nonlocal priors (e.g., nonlocal TV) would be necessary

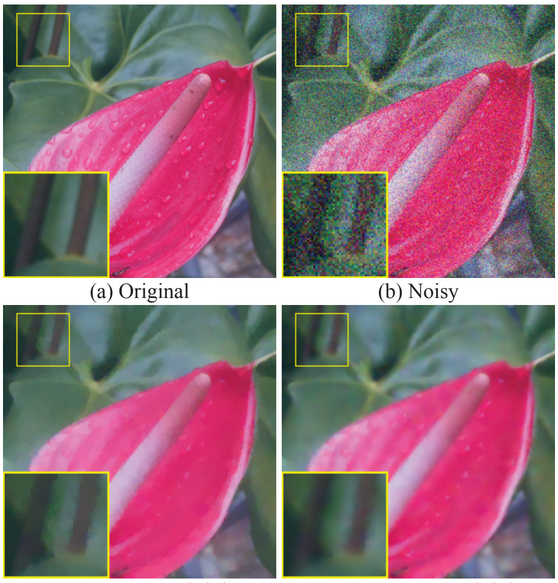

(a) Original (b) Noisy

(c) TV: $\mu = J_{\mathrm{TV}}(\mathbf{v})/4$ PSNR=29.75, CIEDE=3.087 (d) TGV: $\mu = J_{\mathrm{TGV}}(\mathbf{v})/20$ PSNR=30.23, CIEDE=3.032

Fig. 2. Gaussian denoising results using a natural color image.

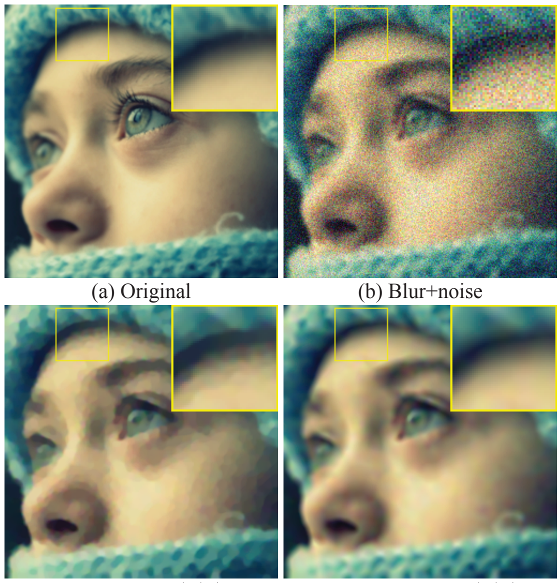

(a) Original (b) Blur+noise

(c) TV: $\mu = J_{\mathrm{TV}}(\mathbf{v})/3.5$ PSNR=31.43, CIEDE=3.346 (d) TGV: $\mu = J_{\mathrm{TGV}}(\mathbf{v})/30$ PSNR=31.71, CIEDE=3.250

Fig. 3. Deblurring results using a natural color image.

ing optimization problems associated with TV constraint (i.e., replacing $C_{\mathrm{TGV}}^{\alpha,\eta}$ by the TV constraint), we also use the primal-dual splitting algorithm [15] with epigraphical projection techniques proposed in [5]. The parameters γ_1 and γ_2 in Algorithm 3.1 are chosen as 0.01 and $1/(12\gamma_1)$, and we set the stopping criterion as $\frac{\|\mathbf{u}^{(n+1)}-\mathbf{u}^{(n)}\|_2}{255} \leq 0.002$. The weight α in the TGV constraint is fixed to 0.5 in all the following experiments.

4.1. Denoising

We first consider a simple Gaussian denoising problem (thus $\mathbf{\Phi} = \mathbf{I}$ in (11)), where test images are contaminated by an additive white Gaussian noise with standard deviation $\sigma = 25.5$.

The results using a grayscale synthesized image with various μ are shown in Fig. 1, where we use $J_{\mathrm{TV}}(\mathbf{v}) := \|\mathbf{Dv}\|_{1,2}^{2M}$ and $J_{\mathrm{TGV}}(\mathbf{v}) := \alpha\|\mathbf{Dv}\|_{1,2}^{2M} + (1-\alpha)\|\mathbf{GDv}\|_{1,2}^{3M}$ ($\mathbf{v}$ is a given noisy image) for choosing μ. For objective evaluation, their PSNR [dB] and SSIM [19] are also presented.[6] As we expected, the smaller μ results in a smoother image in both cases of TV and TGV. The staircasing effect appears in the resulting images by using the TV constraint even if we choose a very small μ (see Fig. 1(d)). By contrast, gradation is well reconstructed by using the TGV constraint (see Fig. 1(g) and (h)).

We also examine the denoising capability of the TGV constraint using a natural color image[7] (Fig. 2), where μ is adjusted to maximize the resulting PSNR ($J_{\mathrm{TV}}(\mathbf{v})/4$ for TV and $J_{\mathrm{TGV}}(\mathbf{v})/20$ for TGV). Here CIEDE2000 [20] is adopted for color quality assessment.[8] One sees that the use of the TGV constraint nicely resolves smooth regions, so that the resulting image indicates better PSNR and CIEDE2000.

4.2. Deblurring

Second we apply the TGV constraint to a deblurring problem, i.e., $\mathbf{\Phi}$ in (11) being a blur operator. Here, a natural color image[9] is blurred by the 5×5 Gaussian kernel with standard deviation 2, and then a white Gaussian noise is added ($\sigma = 25.5$).

The results are given in Fig. 3 with their PSNR and CIEDE2000. Again, we manually adjust μ to achieve the best performance in the sense of PSNR ($J_{\mathrm{TV}}(\mathbf{v})/3.5$ for TV and $J_{\mathrm{TGV}}(\mathbf{v})/30$ for TGV). We observe that the use of the TGV constraint significantly reduces the staircasing effect (PSNR and CIEDE2000 are also improved).

5. CONCLUDING REMARKS

We have proposed a novel use of TGV, i.e., the TGV constraint, with an efficient optimization framework. The proposed framework handles a very general optimization formulation, that is, the minimization of the sum of possibly nonsmooth convex functions over the TGV constraint and other convex constraints. We have illustrated the TGV constraint over several image restoration applications.

Even though we focused on the single use of the TGV constraint as a prior in the presented applications, it can be used together with other priors, such as a color-line prior for color artifact reduction [21], which would compensate for the shortcomings of TGV. The TGV constraint is also applicable to non-Gaussian noise contamination scenarios, for example, impulsive noise [22, 23] and Poisson noise [24, 25, 26], with suitable data-fidelity design. Other than that, it is interesting to utilize the TGV constraint for cartoon-texture decomposition, as studied in [27, 28, 29, 30].

for producing state-of-the-art results, developing techniques for local priors, such as TV and TGV, is still important, for example, for the following reasons: i) local priors are free from chicken-and-egg self-similarity evaluation such as block matching, so that it can be readily used in various restoration scenarios; and ii) initial estimation required for nonlocal priors is usually executed by local priors, which affects the performance of nonlocal priors.

[6] PSNR is defined by $10\log_{10}(255^2 MN/\|\mathbf{u}-\mathbf{u}_{\mathrm{org}}\|_2^2)$ and SSIM by [19, (13)]. For both criteria, a higher value indicates a better quality.

[7] `http://r0k.us/graphics/kodak/andwww.mayang.com/textures`

[8] CIEDE2000 is known as a better criteria for the evaluation of color quality than PSNR (a smaller value indicates a higher quality).

[9] cc licensed (BY) flickr photo by ˆ@ˆina (Irina Patrascu): `http://flickr.com/photos/angel_ina/3201337190/`

6. REFERENCES

[1] L. I. Rudin, S. Osher, and E. Fatemi, "Nonlinear total variation based noise removal algorithms," *Phys. D*, vol. 60, no. 1-4, pp. 259–268, 1992.

[2] A. Chambolle, V. Caselles, D. Cremers, M. Novaga, and T. Pock, "An introduction to total variation for image analysis," in *Theoretical Foundations and Numerical Methods for Sparse Recovery*, pp. 263–340. De Gruyter, 2010.

[3] P. L. Combettes and J.-C. Pesquet, "Image restoration subject to a total variation constraint," *IEEE Trans. Image Process.*, vol. 13, no. 9, pp. 1213–1222, 2004.

[4] J. M. Fadili and G. Peyré, "Total variation projection with first order schemes," *IEEE Trans. Image Process.*, vol. 20, no. 3, pp. 657–669, 2011.

[5] G. Chierchia, N. Pustelnik, J.-C. Pesquet, and B. Pesquet-Popescu, "Epigraphical projection and proximal tools for solving constrained convex optimization problems: Part I," *CoRR*, vol. abs/1210.5844, 2012.

[6] G. Chierchia, N. Pustelnik, J.-C. Pesquet, and B. Pesquet-Popescu, "An epigraphical convex optimization approach for multicomponent image restoration using non-local structure tensor," in *Proc. IEEE Int. Conf. Acoust., Speech, and Signal Process. (ICASSP)*, 2013, pp. 1359–1363.

[7] K. Bredies, K. Kunisch, and T. Pock, "Total generalized variation," *SIAM J. Imag. Sci.*, vol. 3, no. 3, pp. 92–526, 2010.

[8] S. Setzer, G. Steidl, and T. Teuber, "Infimal convolution regularizations with discrete ℓ_1-type functionals," *Commun. Math. Sci*, vol. 9, no. 3, pp. 797–827, 2011.

[9] K. Bredies, "Recovering piecewise smooth multichannel images by minimization of convex functionals with total generalized variation penalty," SFB-Report, 2012.

[10] T. Valkonen, K. Bredies, and F. Knoll, "Total generalized variation in diffusion tensor imaging," *SIAM J. Imag. Sci.*, vol. 6, no. 1, pp. 487–525, 2013.

[11] K. Bredies and M. Holler, "A TGV regularized wavelet based zooming model," in *Scale Space and Variational Methods in Computer Vision*, Lecture Notes in Computer Science, pp. 149–160. Springer Berlin Heidelberg, 2013.

[12] T. Miyata, "L infinity total generalized variation for color image recovery," in *Proc. IEEE Int. Conf. Image Process. (ICIP)*, 2013, pp. 449–453.

[13] D. Ferstl, C. Reinbacher, R. Ranftl, Matthias Rüther, and H. Bischof, "Image guided depth upsampling using anisotropic total generalized variation," in *Proc. IEEE ICCV*, 2013.

[14] S. Ono and I. Yamada, "Decorrelated vectorial total variation," in *Proc. IEEE Conf. Comput. Vis. Pattern Recognit. (CVPR)*, 2014, to appear.

[15] L. Condat, "A primal-dual splitting method for convex optimization involving Lipschitzian, proximable and linear composite terms," *J. Optim. Theory Appl.*, vol. 158, no. 2, pp. 460–479, 2013.

[16] B. C. Vu, "A splitting algorithm for dual monotone inclusions involving cocoercive operators," *Adv. Comput. Math.*, vol. 38, no. 3, pp. 667–681, 2013.

[17] J. J. Moreau, "Fonctions convexes duales et points proximaux dans un espace hilbertien," *C. R. Acad. Sci. Paris Ser. A Math.*, vol. 255, pp. 2897–2899, 1962.

[18] H. Stark and Y. Yang, *Vector Space Projections, a Numerical Approach to Signal and Image Processing, Neural Nets and Optics.*, Wiley Series in Telecommunications and Signal Processing. John Wiley & Sons, Inc., 1998.

[19] Z. Wang, A. C. Bovik, H. R. Sheikh, and E. P. Simoncelli, "Image quality assessment: from error visibility to structural similarity," *IEEE Trans. Image Process.*, vol. 13, no. 4, pp. 600–612, 2004.

[20] G. Sharma, W. Wu, and E. N. Dalal, "The CIEDE2000 color-difference formula: Implementation notes, supplementary test data, and mathematical observations," *Color Res. Appl.*, vol. 30, no. 1, pp. 21–30, 2005.

[21] S. Ono and I. Yamada, "A convex regularizer for reducing color artifact in color image recovery," in *Proc. IEEE Conf. Comput. Vis. Pattern Recognit. (CVPR)*, 2013, pp. 1775–1781.

[22] J. Yang, Y. Zhang, and W. Yin, "An efficient TVL1 algorithm for deblurring multichannel images corrupted by impulsive noise," *SIAM J. Sci. Compt.*, vol. 31, no. 4, pp. 2842–2865, 2009.

[23] R. H. Chan, Y. Dong, and M. Hintermüller, "An efficient two-phase L^1-TV method for restoring blurred images with impulse noise," *IEEE Trans. Image Process.*, vol. 19, no. 7, pp. 1731–1739, 2010.

[24] M. A. T. Figueiredo and J. M. Bioucas-Dias, "Restoration of Poissonian images using alternating direction optimization," *IEEE Trans. Image Process.*, vol. 19, no. 12, pp. 3133–3145, 2010.

[25] M. Carlavan and L. Blanc-Fèraud, "Sparse Poisson noisy image deblurring," *IEEE Trans. Image Process.*, vol. 21, no. 4, pp. 1834–1846, 2012.

[26] S. Ono and I. Yamada, "Poisson image restoration with likelihood constraint via hybrid steepest descent method," in *Proc. IEEE Int. Conf. Acoust., Speech, and Signal Process. (ICASSP)*, 2013, pp. 5929–5933.

[27] L. Vese and S. Osher, "Modeling textures with total variation minimization and oscillating patterns in image processing," *J. Sci. Comput.*, vol. 19, no. 1, pp. 553–572, 2003.

[28] J.-F. Aujol, G. Gilboa, T. Chan, and S. Osher, "Structure-texture image decomposition - modeling, algorithms, and parameter selection," *Int. J. Comput. Vis.*, vol. 67, no. 1, pp. 111–136, 2006.

[29] V. Duval, J. F. Aujol, and L. Vese, "Mathematical modeling of textures : application to color image decomposition with a projected gradient algorithm," *J. Math. Imag. Vis.*, vol. 37, no. 3, pp. 232–248, 2010.

[30] S. Ono, T. Miyata, and I. Yamada, "Cartoon-texture image decomposition using blockwise low-rank texture characterization," *IEEE Trans. Image Process.*, vol. 23, no. 3, pp. 1128–1142, 2014.